de Haas–van Alphen effect and the band structure of UGe_3

A. J. Arko and D. D. Koelling
Argonne National Laboratory, Argonne, Illinois 60439
(Received 29 July 1977)

de Haas–van Alphen measurements, band-structure calculations, and a model of the Fermi surface are presented for UGe_3. This system is representative of the $L1_2$ structured UX_3 compounds (where X is a group-III or -IV element) and is characterized as a spin-fluctuation system. Excellent agreement (considering the complications) is obtained between data and calculations. A large narrow peak in the density of states is found at the Fermi energy and is believed responsible for the nearly magnetic phenomena. Large mass enhancements are indicated. By studying UGe_3, we attempt to provide some insight into the systematics of these UX_3 systems.

I. INTRODUCTION

The systems with the formula UX_3, where X is a group-III or -IV element, tend to crystallize in the $L1_2$ (or Cu_3Au type) structure[1] shown in Fig. 1(a). Focussing on the group-IV series, one sees that the lattice constant increases as one moves down the series from Si to Pb (USi_3: 4.035 Å, UGe_3: 4.206 Å, USn_3: 4.626 Å, and UPb_3: 4.792 Å). Simultaneously, the electronic specific-heat γ values rise[2] (Si: 14.0, Ge: 20.4, and Sn: 170 all in mJ/mole $°K^2$) as does the paramagnetic susceptibility[3] (Si: 700, Ge: 1300, Sn: 1833 all in 10^{-6} emu/mole). In general, it appears that the 5*f* orbitals exhibit a more localized or narrow-band-like behavior as one proceeds down the Periodic Table for the choice of X element: USi_3 is a more or less normal metal; UGe_3 is characterized as a spin-fluctuation system[3]; USn_3 could be called a superpalladium system which can probably be induced to go antiferromagnetic with alloying[4]; and UPb_3 undergoes an antiferromagnetic transition[5] at 32 °K.

The lattice constants are sufficiently large that the uranium spacings preclude a direct 5*f*-5*f* orbital interaction. Thus, these itinerant systems are anomalous on the Hill plots[6] which relate interactinide spacings to localized or itinerant behavior. This implies that if there are occupied 5*f* orbitals (which we find) there must be at least one other mechanism operative in creating itinerant-electron behavior. These mechanisms are, of course, especially interesting because they are the ones that will persist in the magnetic actinide systems.

Our previous experience[7-11] with URh_3 and UIr_3 had implicated the formation of a strong *d*-*f* bond, but the above nontransition-metal systems do not exhibit any *d* character on the X sites. The natural supposition to make in the case of these UX_3 systems is that a *p*-*f* bond is formed, especially as three *f* electrons can produce the same angular variation as three *p* electrons. While the formation of *p*-*f* bonds is no doubt of great significance (most of our states at the Fermi energy are formed in this way), one must consider the possibility that this is not the dominant mechanism. These *p*-*f*

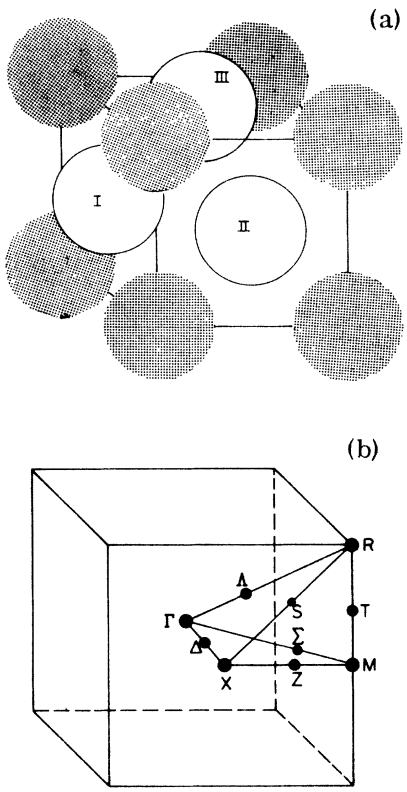

FIG. 1. $L1_2$ (Cu_3Au type) crystal structure (a) and Brillouin zone (b). The Cu_3Au structure can easily be visualized as a face-centered-cubic lattice in which the face-centered sites (I, II, and III) are occupied by Cu and the simple cubic (i.e., corner) sites are occupied by Au.

bonds, after all, will be relatively weak since they will be π bonds in this geometry. Further, the lattice constants follow reasonably well those predicted by merely summing the atomic radii,[12] but progressively falling further below the predicted values as one moves down the Periodic Table. Since the atomic radius of the X atom is tied to the size of the p orbital, one might naively expect a *larger* f-p overlap and thus then predict a trend opposite to that observed using the f-p bond model.

Thus it is appropriate to also consider the only other orbitals with significant occupancy near the Fermi energy: the uranium d orbitals. If there were to be a significant U-d, U-f interaction, this would be diminished as one proceeded from USi_3 to UPb_3 due to the increased separation and would thus provide a plausible explanation for the observed trend. We, however, will argue that this is not the case.

The key lies in the fact that Si is a much smaller ion than U while Pb is somewhat larger. (Since one should probably be using the negative ionic radius, the crossover should most likely occur between the Ge and the Sn compound. This will be born our by our calculations.) Thus, one might expect that the interactions between the X atoms would dramatically increase as one progresses down the Periodic Table. One assumes that this interaction would compete with the U-X interaction. Further, as the spatial extent of the p orbitals increases, the intra-atomic Coulomb interaction of these orbitals ought to decrease allowing greater charge transfer. This would result in a reduced shielding for the $5f$ orbitals causing them to be contracted and thereby more localized.

It is always possible to make speculations but it is a useless exercise unless one can utilize experimental data to distinguish between some of the alternatives. Our "experimental data" are the band-structure results presented in Sec. III. However, to have any confidence at all in the calculational results, they must be relatable to actual laboratory experimental data on the systems. The comparatively simplest and most precise such data are the de Haas–van Alphen frequencies. We are very fortunate that UGe_3 single crystals can be prepared with quality adequate to successfully perform the de Haas–van Alphen measurements. These are reported in Sec. II. Finally, in Sec. IV we discuss the significance of our results to the UX_3 class of systems.

II. EXPERIMENTAL

A. Sample preparation

Single crystals of UGe_3 were prepared by precipitation from a Bi flux. Briefly, this consists of heating a mixture of Bi with ≈ 4-at.% UGe_3 in a tungsten crucible to ≈ 1000 °C in a pure argon atmosphere. The temperature is then cooled slowly (≈ 3 °C/h) to 400 °C. The solubility of UGe_3 in Bi decreases with temperature and UGe_3 precipitates out. Below 400 °C very little additional precipitation occurs and the cooling rate is increased to 100 °/h. The solid Bi is dissolved away in concentrated HNO_3 leaving behind small crystals (maximum length ≈ 4 mm) of UGe_3. The shape of the crystals is that of parallelepipeds with the edges corresponding to $\langle 100 \rangle$ axes. The resistance ratios of some representative crystal were as high as 450 indicating very little solution of Bi or other impurities in UGe_3. The measured Dingle temperature was ≈ 0.4 °K.

Because of the small size of the crystals and excellent crystallographic perfection, it was only necessary to pick a sample whose size best fits our equipment (≈ 1 mm^3) with no cutting or etching necessary.

B. Measurement

The high purity of the specimens enabled us to observe orbits with effective masses (m^*) greater than 4 in our 70-kG superconducting magnet. The small size of the specimens resulted in field homogeneity across the specimen of ≈ 2 ppm. The large masses also mandated that the work be done at temperatures of ≈ 0.5 °K. This was accomplished via ^{3}He evaporative cooling.

Measurements were done utilizing the usual field-modulation technique.[13] A rotating probe capable of two degrees of freedom[14] was used to change the crystal axis relative to $\vec{H}$. Because of the two degrees of freedom it was possible to orient the sample *in situ* using the de Haas–van Alphen (dHvA) effect itself; thus only one mounting of the specimen was necessary for both planes [(100) and (110)] measured. We estimate the accuracy of orientation to be within 1°. The spectral content of the dHvA signal was analyzed by an online PDP-11/20 minicomputer programmed to perform fast or slow Fourier transforms.[15] The dHvA signal proved to be exceedingly complex (up to 20 frequencies for some orientations) due to the large harmonic content (up to the seventh) of the small, low-mass frequencies, so that the computer capability was absolutely essential in sorting out the data.

Nearly all masses were of necessity measured in ^{3}He below 1 °K. Temperature was determined by measuring the ^{3}He vapor pressure with a Baratron electronic monometer. A 6-mm-diam static line extended from the top of the Dewar to just above the ^{3}He to avoid pressure drops in a pumping line. By always taking data in decreasing tem-

perature steps and by allowing about a minute for thermal equilibrium, effective masses of value $m^* < 3$ could be measured to 2%. Above this value the errors increased because of the small amplitude of the signal and small temperature range over which it was observed.

C. Results and Fermi-surface topology

The dHvA spectrum for UGe_3 is plotted on a logarithmic scale in Fig. 2 for the (100) and (110) planes. The orbital effective masses are given in Table I for the various orbits measured. The complex nature of the dHvA spectrum is evident. It was particularly difficult to separate the γ_i (except for γ_6) and ρ_1 frequencies since for many field directions these frequencies nearly coincided with the various harmonics of the low-mass μ_i frequencies.

The most readily interpretable frequency branches are those labeled ρ_1 and ρ_2. Both are due to surfaces that have the symmetry of either Γ or R in the simple cubic Brillouin zone. From the band-structure calculations to be discussed in Sec. III it is evident that both frequencies are due to hole surfaces centered at R and coming from bands 8 and 9 (see Fig. 4 in Sec. III). (In our initial UGe_3 correspondence,[16] we had assumed that ρ_1 was centered at Γ.) The data indicate that these surfaces

TABLE I. Orbital effective masses for several orbits and orientations in UGe_3.

Frequency branch	Field direction	Mass (m^*/m_0)
γ_6	[111]	2.25 ± 0.05
ρ_1	[100]	3.75 ± 0.1
ρ_2	[100]	4.31 ± 0.1
$\mu_{2,3}$	[100]	0.42 ± 0.02
μ_1	[100]	1.93 ± 0.02
γ_4	[100]	0.80 ± 0.02
γ_7	[100]	1.10 ± 0.02

are nearly spherical with very slight bulges in the ⟨111⟩ directions. The bulges are larger in ρ_1 than in ρ_2. The data are incomplete for ρ_2 undoubtedly because of the large effective mass near ⟨110⟩. The signal for ρ_2 is strongest at ⟨100⟩($m^* = 4.1$) and gradually gets weaker toward ⟨111⟩ until it disappears completely within ≈10° from ⟨110⟩. It is seen from Table I that these two surfaces have the heaviest orbital masses in UGe_3 and probably contribute the bulk of the f-electron density at the Fermi surface.

Frequency branches μ_i (which have the lowest orbital effective masses in the UGe_3 spectrum) also lend themselves to relatively easy interpretation. They are due to a set of nearly circular, lenslike surfaces centered either at M or at X. It was again necessary to resort to band calculations (see discussion below) to determine their location. Band 10 in Fig. 4 is seen to cross E_F at a number of points in the Brillouin zone. Specifically, one of the crossings is at M where indeed a lenslike electron pocket is obtained. Figure 3 shows the

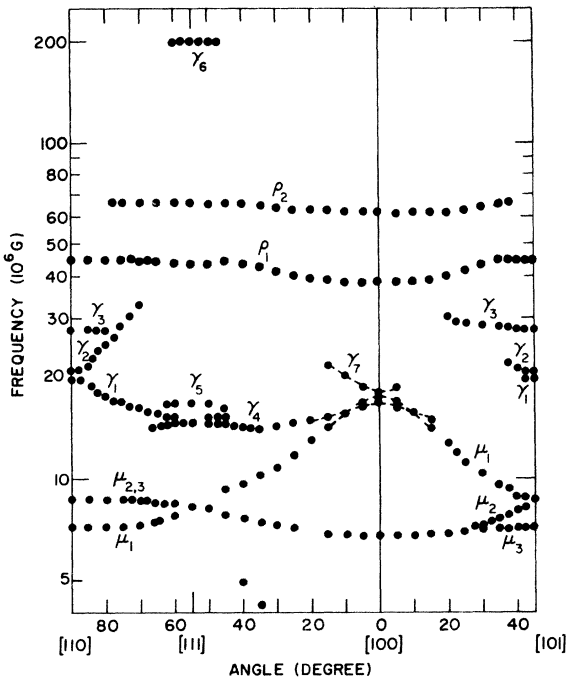

FIG. 2. Angular variation of the observed de Haas–van Alphen frequencies in the (100) and (110) planes.

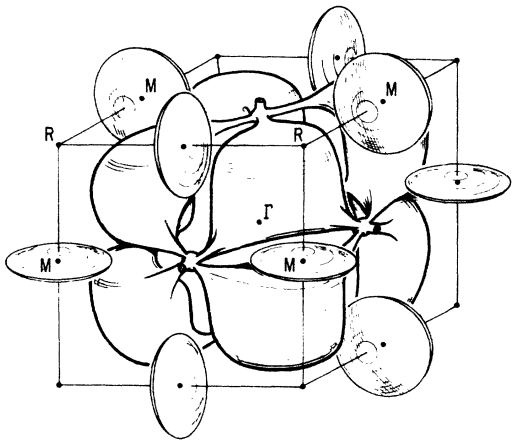

FIG. 3. Proposed topology of the electron Fermi surfaces.

Fermi-surface model which is topologically consistent with the data and with band 10. The lenses in question are situated at the points M. We will refer to them as the μ surfaces. The experimentally determined lens has an average diameter of 0.244 a.u., while the maximum thickness of the disk along $\langle 100 \rangle$ is 0.094 a.u. Band calculations are predicting a maximum diameter of ≈ 0.45 a.u. for the lens. The problems associated with this will be discussed below.

The γ_i branches are undoubtedly part of a complex, multiply-connected surface. In this case neither the symmetry nor the topology could be determined unambiguously from experimental data alone. With considerable feedback between models obtained from analysis of the data and the band calculations, we believe we have determined a model of the Fermi surface having the correct topology. The surface is shown in Fig. 3 as the large open surface centered at Γ. We will refer to it as the γ surface. Direct comparison between data and calculations for this surface are not yet quantitative because of the extreme sensitivity of band 10 to the exact crystal potential and the fitting problems to be described below. Branches γ_1 and γ_4 can be followed for a longer range of angles than the remaining γ_i branches and are thus believed to correspond to orbits on the thick portions of the multiply-connected surface which are centered at Λ, rougly midway on the Γ-R line. The degeneracy at [111] supports this interpretation. However, because of the multiplicity of frequencies (including harmonics) near [111], it is not totally unambiguous that γ_1 and γ_4 are separate branches. In all likelihood they are, however. We believe that each branch cuts off just beyond [111] and has a turning point at [111], where γ_1 and γ_4 are degenerate. The cross-sectional areas of these orbits are roughly comparable to the largest area of the lens but this is not yet obtained in band 10.

The situation at [110] is also not totally clear. If γ_1 has been correctly interpreted as corresponding to orbits centered on the Γ-R line, then γ_1 should be degenerate with a second branch at [110]. We do not observe this degeneracy although the connectivities of γ_1 and γ_2 are still open to some questions since the third harmonic of μ_1 falls precisely in the region of interest, thus washing out some information.

The remaining γ_i branches are undoubtedly due to hole or neck orbits on this complex γ surface, but we have not yet been able to identify them, with the exception of γ_6. We feel confident that this very large frequency (nearly equal to the cross-sectional area of the zone face) is due to an orbit which goes through six necks (at X) and encompasses six zones. The area of this large orbit is not so sensitive to small changes in the γ surface, and in this case semiquantitative agreement is obtained with band structure. Frequency branch γ_5 can tentatively be identified as due to an orbit on the inside of the γ surface and passing behind three X points.

The fact that the surfaces at Λ bridge across and make contact with the X point in the Brillouin zone was not immediately obvious either from the data or the band structure. The problem became particularly confus. when a magnetoresistance experiment[17] failed show evidence for open orbits for $\vec{J} \parallel \langle 100 \rangle$ and $\vec{H} \parallel \langle 110 \rangle$. We had considered the possibility that the large γ_6 orbit is due to magnetic breakdown possibly involving the lenses in some unusual and unknown fashion. (Both γ and μ are electron surfaces.) However, an investigation revealed no deviation from the normal amplitude dependence for γ_6. This fact leaves the six-zone orbit (and the existence of necks at the X point) as the only configuration which can accommodate and explain the large cross-sectional area of γ_6. In order to explain the lack of open orbits, then, it is necessary that the bridging of the γ surface occurs some distance behind the X point, as drawn in Fig. 3. That is, the locus of points of intersection of the γ surface with a (110) plane containing two X points must not be continuous between the two Brillouin-zone faces.

The small necklike surfaces centered at the X points should support extremal orbits and hence dHvA frequencies of the order 1×10^6 Gauss for $\vec{H} \parallel \langle 100 \rangle$. None were observed although it should be pointed out that it is very difficult to observe frequencies $F < 1 \times 10^6$ with the field-modulation technique. Frequency branch γ_7 has the correct symmetry but it is far too large to be identified with this orbit.

It is not clear whether the necklike portion of the γ surface which extends approximately along the Λ-X line can support extremal orbits. Some weak frequencies were observed at two angles $\approx 40°$ from [100] in the (110) plane but these data are too sparse to make any identification.

III. THEORETICAL ELECTRONIC STRUCTURE

We have calculated the band structure of UGe_3 using a variant of the relativistic augmented plane wave method[10,18,19] applied to a crystal potential constructed from an overlapping charge-density model. The exchange-correlation functional of Gunnarsson, Lundqvist, and Wilkins was used.[20] This yields the form

$$V_{xc} = \beta(\rho) V_x(\rho), \tag{1}$$

where the V_x is the usual $\rho^{1/3}$ form

$$V_x = (-2/\pi)(3\pi^2\rho)^{1/3}, \tag{2}$$

and β is a density-dependent X_α-like parameter

$$\beta(\rho) = 1 + 0.0545 r_s \ln(1 + 11.4/r_s),$$
$$r_s = (3/4\pi\rho)^{1/3}. \tag{3}$$

Our prime motivation for using this functional is that it automatically provides a coefficient $\approx \frac{2}{3}$ in the vicinity of the uranium atom, and somewhat larger in the vicinity of the Ge atom as required, rather than having to use a different α for each region of space.

Within the overlapping charge-density model, there exist a number of parameters in the form of the configurations assumed for the constituent atoms. For transition and rare-earth metals, this reduces merely to the relative populations of s and d orbitals and is easily managed by well-known rules-of-thumb (i.e., as one increases the exchange coefficient or decreases the number of d electrons in the atomic configuration, the d bands will move to a lower energy and broaden). However, when one is dealing with a compound, the number of possibilities is greatly increased and can require an inordinate number of calculations as we have experienced for URh_3.[7] Not being ready to perform a full self-consistent calculation, we have instead chosen to utilize a pseudo-self-consistency in assigning the occupation numbers for an overlapping charge-density model calculation. The scheme is an oversimplified treatment of ideas originating with the renormalized atom[21] and atomic sphere approximation[19,22] approaches. The basic requirement of the scheme is that one can roughly locate the position of the bands arising from a given atomic character by an examination of the single-site solutions. The bottom of the band is found from the Wigner-Seitz requirement that the radial function have zero derivative at the Wigner-Seitz radius. (The choice of Wigner-Seitz radii will be discussed below.) The "center of mass" for the band is obtained from the requirement that the logarithmic derivative equal that of the Neuman function, or, roughly, $-(l+1)/R$. The top of the band is obtained from the requirement that the radial function go to zero. Given these reference points, we can then take the step of arbitrarily drawing a partial density of states with the additional requirement that it accommodate the proper number of electrons. This cavalier approach is justifiable on the basis that one should not try to push the overlapping-charge-density (OCD) model beyond ± 0.25 for the orbital occupation numbers of the s, p, and d electrons and ± 0.1 for the occupation number of the f electrons, due to the greater sensitivity of the potential to the f occupation. Any attempt to further refine the configurations used in the atomic calculations beyond this is really just a parametrization scheme as the OCD model does not incorporate the other distortions present in the crystal. This, however, is adequate for our purpose. Once one has created the model density of states one can then determine a Fermi energy and, from the integrated partial density of states, a new set of occupation numbers. This can be repeated until the calculated occupation numbers agree with those used in the creation of the potential, a form of pseudo-self-consistency.

A critical choice to be made is, of course, the radii to be used in the prescription. The choice is easy in a pure metal: one uses the Wigner-Seitz radius. The procedure we have followed is to require

$$\tfrac{4}{3}\pi(R_U^3 + 3R_{Ge}^3) = \Omega = a^3, \tag{4}$$

and scale them according to the size of the muffin-tin radii

$$R_U/R_{Ge} = R_U^{MT}/R_{Ge}^{MT}. \tag{5}$$

The muffin-tin radii were assigned within the potential generating code by the requirement that the atomic charge within the uranium sphere and *one* germanium sphere should be a maximum subject to the condition of nonoverlapping. An alternate procedure is to follow the prescription of Slater[23] that the ionic radius be assigned at the principal maximum of the outer orbital and then the radii scaled according to these ionic radii. It is a consequence of either choice that the radii used will vary from iteration to iteration.

This pseudo-self-consistent-field procedure was begun with $U^0 f^3 d^2 s^1$ and $Ge^0 s^2 p^2$. It yielded instead the results $U^{3+} f^2 d^1$ and $Ge^- s^2 p^3$. Several interesting features were observed along the way. Following the above prescription, the initial neutral configuration resulted in muffin-tin radii with the uranium much larger than the germanium. The rms deviation from a muffin-tin potential in the interstitial region was large (~0.25 Ry). The final ionic configuration resulted in very nearly equal radii and a potential with a reduced rms deviation (~0.15 Ry) which is nearer that of a typical fcc metal (~0.08 Ry). The Fermi energy found by the model self-consistent-field (SCF) procedure (0.10 Ry) agreed moderately well with that found when the band structure was actually calculated (0.164 Ry). The lattice constant used throughout was 7.9842 a.u. Although this is the room-temperature value, it is not possible to correct it to helium temperature without thermal expansion data. In any case, the error in lattice constant is not one of the major sources of error in our calculations.

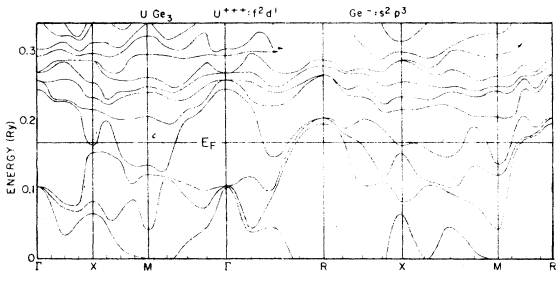

FIG. 4. Band structure calculated for UGe_3. Note that a nonsymmetry line from $X[100]$ to $M[011]$ has been included as well as the standard symmetry directions shown in Fig. 1.

The relativistic-augmented-plane-wave (RAPW) calculations were performed using a variant[10] of the RAPW method which utilized the energy derivative of the radial function (EDRF). The technique has been discussed for the nonrelativistic case elsewhere[18] and the relativistic version is a straightforward generalization of the nonrelativistic case where the angular momentum l is replaced by the relativistic κ (or j). With the EDRF providing a degree of variational freedom for the interior of the muffin-tin spheres, one chooses an energy e_κ^n to set up the radial function and EDRF and then solves a secular equation, rather than plotting determinants. We, in fact, performed two calculations: one with all $e_\kappa^n = 0.10$ Ry (the model SCF Fermi energy), and one with all $e_\kappa^n = 0.16$ Ry, except the uranium p functions which were set at -0.5 Ry. The resultant eigenvalues in the vicinity (± 0.10 Ry) of the Fermi energy differed by less than 0.003 Ry. The uranium p functions were set to the low energy to provide a reasonable representation of the $6p$ band. If this was not done, a poorly converged $6p$ band was found at roughly -0.04 Ry. Such "spurious" bands have been discussed in detail by van Dyke.[24] In any case, this spurious band had no effect in the vicinity of the Fermi energy.

The band structure calculated is shown in Fig. 4. It was calculated using a warped muffin-tin approximation to the overlapping charge-density model using the configurations U^{+3} f^2d^1 and Ge^- s^2p^3 with the Gunnarsson-Lundqvist-Wilkins exchange-correlation parameterization. The warped muffin-tin approximation spherically averages the potential about each site but utilizes the full model potential in the interstitial region. This is not unreasonable at the uranium site which has full cubic symmetry, so one is primarily neglecting small d-d and f-p couplings. It is more severe at the Ge site which has D_{4h} site symmetry, so one is neglecting p-p and s-d couplings as well. For Ge, it is the p-p coupling which will concern us and we will return to this point.

Because of the many anticrossings caused by the overlapping and hybridization of many bands, there is a good deal of (sharp) structure in the bands. Thus, one sees that a Fourier-series fit is doomed to rather large inaccuracies. Nonetheless, we used it to determine a density of states and thereby a Fermi energy of 0.1642 Ry. To provide some check on this value, we then used the somewhat old-fashioned weighted-summation technique and obtained a Fermi energy of 0.1637 Ry. The 43 points at which we calculated the eigenvalues consisted of the 35-point cubic $\pi/4a$ grid plus an additional 8 points at the centers of tetrahedron obtained by dividing the $\frac{1}{48}$th tetrahedron dimensions in half. The 35 points were given weights to provide 95% of the integral and the other eight the remaining 5%. The relative weights within the 35- and 8-point sets are, of course, fixed by geometrical considerations. It is this density of states which is shown in Fig. 5.

The density of states at the Fermi energy is 33 states/(formula–unit spin)(11.4 mJ/mole K^2). This result is very uncertain as one can vary the result considerably (primarily downward) by varying the histogram width and position. The Fourier series yielded 17.5 states (formula–unit spin) with the immediately adjacent peak having the value observed by the histogram technique. In any case, when compared to the experimental value (20.4

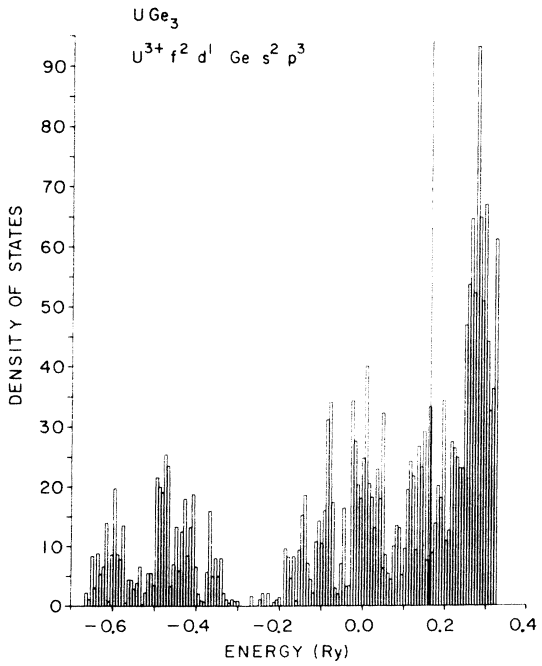

Fig. 5. Total density of states for UGe_3.

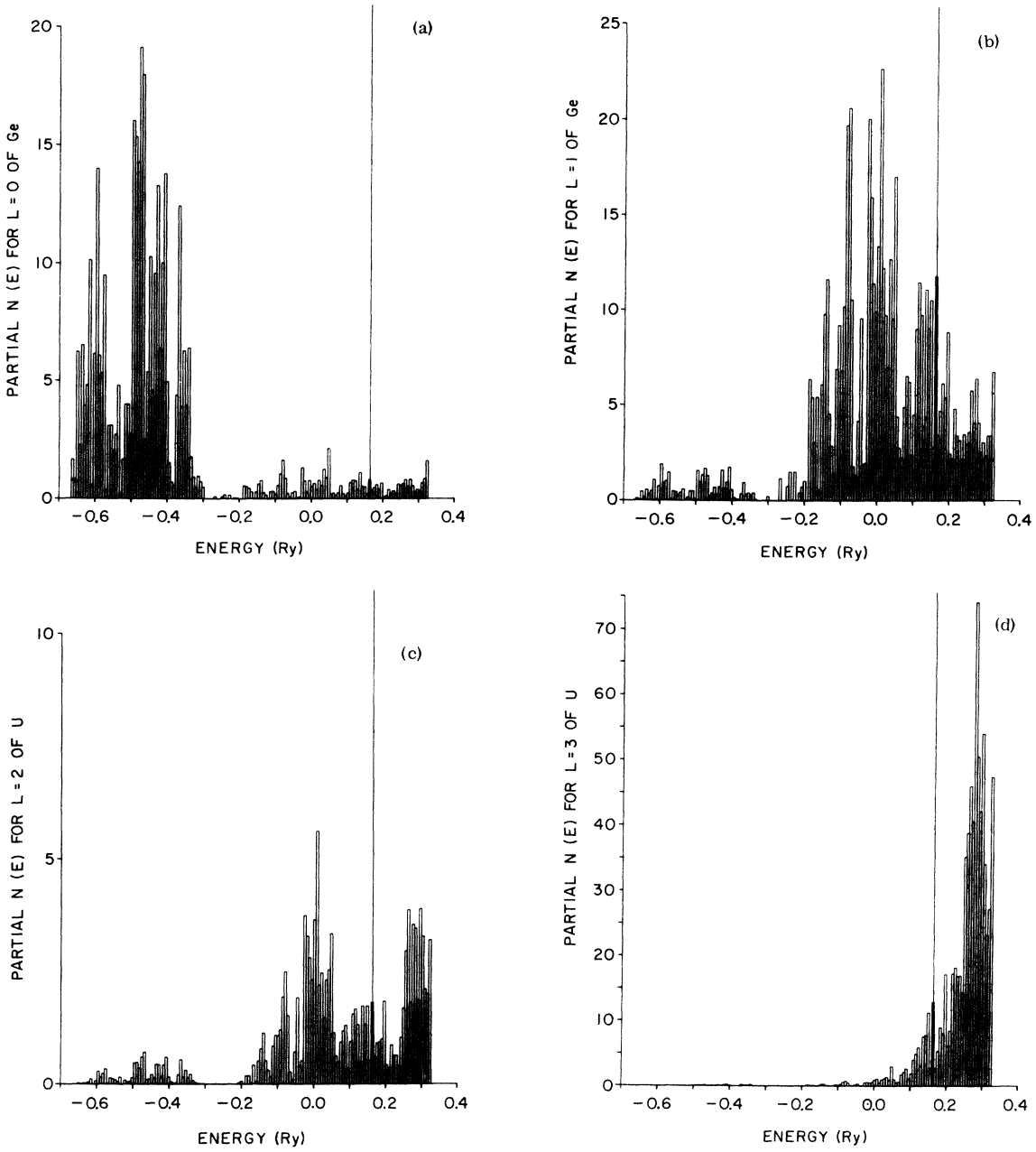

FIG. 6. Partial density of states for: (a) Ge-s; (b) Ge-p; (c) U-d; and (d) U-f character. Weighting is by the "l" character within the muffin-tin spheres and so does not account for charge in the interstitial region. ("l" character was obtained by summing the appropriate two j components.)

mJ/mole K^2), this would imply a large enhancement factor of 2 or more. One should believe these indications of a narrow peak in the density of states. In Fig. 4, one sees a plateaulike structure in bands 7 and 8 along the M-R line. This persists into the zone. Comparison with the de Haas–van Alphen data indicates that these bands should actually be pulled down to a point where this structure is at or just below the Fermi energy (to make ρ_1 and ρ_2 the correct size). This would insure that this density peak falls very near the Fermi energy and that it would be quite narrow.

The so-called l-decomposed densities of states were also calculated using the weighted summation technique. We used only the fractional l character (obtained by summing the results for $\kappa = l$ and

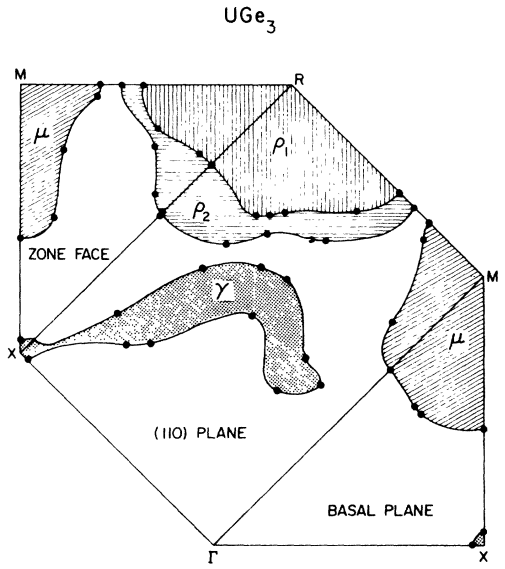

FIG. 7. Intersection of the calculated Fermi surface with the planes bounding the $\frac{1}{48}$th of the Brillouin zone shown in Fig. 1.

$\kappa = -l-1$) within the muffin-tin spheres, i.e., no correction was made for the interstitial region. Thus, for example, the decomposed densities of states will not sum to the density of states and certainly should not be identified with an atomic-orbital character. Nonetheless, these l-character decompositions can aid in understanding how various bands are made up and are presented here as such a *qualitative* guide. In Fig. 6, we show the total Ge-s, Ge-p, U-d, and U-f densities. The U-s and U-p densities have not been shown as they are quite small, consistent with the pseudo-self-consistent model which was used to generate the potential. One notes immediately from Fig. 6(a) that there are three Ge-s bands in the energy range -0.7 to -0.3 Ry which is consistent with our using two s electrons in the Ge configuration. The Ge-p and U-d densities have considerable density at about the zero energy range reminiscent of the d-p bond observed in the actinide-hexafluoride calculations[25] just below the f-p hybrid states. The p-f hybrid states are observed to be just below and at the Fermi energy. The peak in U-f character just below 0.3 Ry is seen *not* to have a large Ge-p character associated with it.

The Fermi surface resulting from this calculation is shown in Fig. 7. To avoid using the Fourier-series representation, this figure was created by graphical interpolation of the RAPW eigenvalues. That is, the bands were plotted along various lines in the Brillouin zone (beside the symmetry lines) and the Fermi-energy crossings were then plotted. These points are shown in Fig. 7 as the black dots. The two hole surfaces at R and the disks at M are easily seen from this figure. The only evidence of the complex structure represented in Fig. 3 is the speckled volume labeled γ. This surface (when completed with the other three sections obtained by rotation) would yield a four armed orbit in the ⟨110⟩ field direction. Although the calculated area is roughly 25% too large (all calculated areas are too large), this orbit should correspond to the 28-MG frequency observed (γ_3).

The hole orbits at R are not only too large but of the wrong shape. They would have roughly the correct size and shape (note the plateau along M-R line in Fig. 4) if we were to raise the Fermi energy roughly 8 mRy. This would, of course, create serious problems for the electron surfaces as the M-centered disks are also already too large. A simple empirical lowering of the Fermi energy for the electron band would be disastrous for then the bridging at X would be lost and we have seen that this bridging is the key to understanding the remaining complex piece, in particular the 200-MG ⟨111⟩ orbit (γ_6). The overall agreement between the calculation and the experiment would be significantly enhanced if the bands were to be raised a few milliRydberg at M and lowered a few milliRydberg at R. To examine the significance of this, we examine the wave-function principal l character tabulated in Table II. [In addition to the data shown, there is slight U s- and d-, and sizable (0.18) Ge s-orbital character mixed into band 10 at the point X. This is probably a more plane-wave-like band. There is also a very small U p- and Ge s-orbital admixture into bands 9 and 10 at M.] Because of the higher f character at R relative to that at M, it might be possible to adjust the

TABLE II. Wave-function principal "l" character of the conduction bands at the high-symmetry points.[a]

$\vec{k}$ point	n	$\epsilon_n(\vec{k})$	$U(f)$	Ge(p)
Γ	8	104	0.50	0.39
	9	104	0.50	0.39
	10	245	0.93	~0
X	8	83	0.37	0.44
	9	152	0.33	0.33
	10	163(5)	···	0.52
M	8	43	0.14	0.56
	9	120	0.44	0.36
	10	136	0.46	0.35
R	8	195	0.79	0.12
	9	203	0.80	0.10
	10	203	0.80	0.10

[a] Energies are expressed in millirydbergs.

results by making the uranium potential more attractive (fewer f's) and the germanium more repulsive (more p's) so a greater attention to self-consistency might be helpful. This is also the direction that the potentials would change if $\beta(\rho)$ were more slowly varying. On the other hand, we have omitted an important interaction for the Ge p states by spherically averaging the potential within the Ge muffin-tin spheres. One might reasonably expect this additional interaction to cause the bands to repel each other which would also be in the desired direction. In any case, it should be remembered that we are discussing rather small changes, on the scale of precision to which a band-structure calculation is to be believed.

IV. DISCUSSION

The gross features of the UGe_3 electronic structure show a great deal of similarity to those observed for the actinide hexaflourides[25]: there are d-p hybrid states below a set of f-p hybrid states in the occupied portion of the conduction bands. Just above the Fermi energy, there is seen a set of states made up mostly of f orbitals with some relatively slight admixture. In the AF_6 (where A is an actinide atom) calculations these could be seen to total 14 states (only not pure f states). This is quite remarkable as the local site environment for the U in the $L1_2$ structure is very different from that in UF_6. (The simplest cluster would be UGe_{12}.)

From this comparison, one might believe that the way to build the UGe_3 electronic structure is to first form the ionic solid $U^{6+}Ge_3^{2-}$ and then allow the electrons to relax back onto the uranium. (This would be quite consistent with the fact that the group-V compounds do not form.) The "crystal-field f levels" of the uranium remain unoccupied, but through the formation of hybrid (bonding) states, lose some of their f-orbital character to the conduction bands at the Fermi energy. Thus, one ends up with a metal which has large ionic bonding present, which is probably what actually holds the system together, and is consistent with the extreme brittleness of the compounds.

If we now return to the questions about the character of the hybrid states, it is useful to consider a set of mixing indicators defined as follows:

$$n(E)\xi_{\nu\nu'}(E) \equiv \sum_{\vec{k}n} f_\nu(\vec{k},n) f_{\nu'}(\vec{k},n)\delta(E - E_n(\vec{k})), \quad (6)$$

$$f_\nu(\vec{k},n) = \sum_i \sum_\kappa \sum_\mu A^*_{i\kappa\mu}(\vec{k}n) A_{i\kappa\mu}(\vec{k}n) , \quad (7)$$

where ν indicates both the atomic type and an "l" value gotten by summing $\kappa = l$ and $-(l+1)$ in f_ν.

The $A_{i\kappa\mu}(\vec{k},n)$ are the wave-function expansion coefficients

$$\psi(\vec{k},n) = \sum_{\kappa\mu} A_{i\kappa\mu}\phi_{\kappa\mu},$$
$$\int_{r \le R_{MT}} \phi_{\kappa\mu}\phi_{\kappa'\mu'} d^3r = \delta_{\kappa\kappa'}\delta_{\mu\mu'}, \quad (8)$$

so that $f_\nu(\vec{k},n)$ are the fraction of the wave-function density with that "l" character about a given site. As a check on these definitions, note that

$$n(E) = \sum_{\vec{k},n} \delta(E - E_n(\vec{k})), \quad (9)$$

$$n_\nu(E) = \sum_{\vec{k},n} f_\nu(\vec{k},n)\delta(E - E_n(\vec{k})). \quad (10)$$

Also note that, as we have divided out the density of states, $\xi_{\nu\nu'}$ will always be less than unity. These quantities are shown in Fig. 8 for the three cases of interest. One notes a strong peaking of the Ge-p, U-f mixing about the Fermi energy. The U-d, Ge-p mixing is not so predominant but does peak around $E = 0$. The U-d, U-f admixture is seen to be very minimal. From these we can see both the d-p bonding states lying below the f-p states and the inapplicability of a U-d–U-f bonding model.

We are now left with the following picture for these systems: (a) There is a large charge transfer with the remaining occupied orbitals in higher angular momentum states. This gives an ionic bonding in a metal with the remaining metallic electrons not able to fully screen the interactions. (b) A valence-band complex is formed of U-d, Ge-p hybrid states. (c) The conduction bands are formed of U-f, Ge-p hybrid states. (d) A first crystal-field-like U-f state is found roughly $1\frac{1}{2}$ eV above the Fermi energy. (The crystal-field-like label should not be taken too seriously.) The systematic trend toward a more localized orbital behavior as one goes down the Periodic Table in the group-IV elements is therefore due to the increasingly successful competition of the X-p, X-p interactions.

As for the group-III compounds, one should note that the atomic radii are larger than those of the group-IV elements of the same row. This should result in the group-III elements exhibiting magnetic properties somewhat sooner. This appears to happen in that an antiferromagnetic transition is already observed in UIn_3.[3]

The rather good agreement of the de Haas–van Alphen data and our calculations has led us to believe that we do have a basic understanding of the

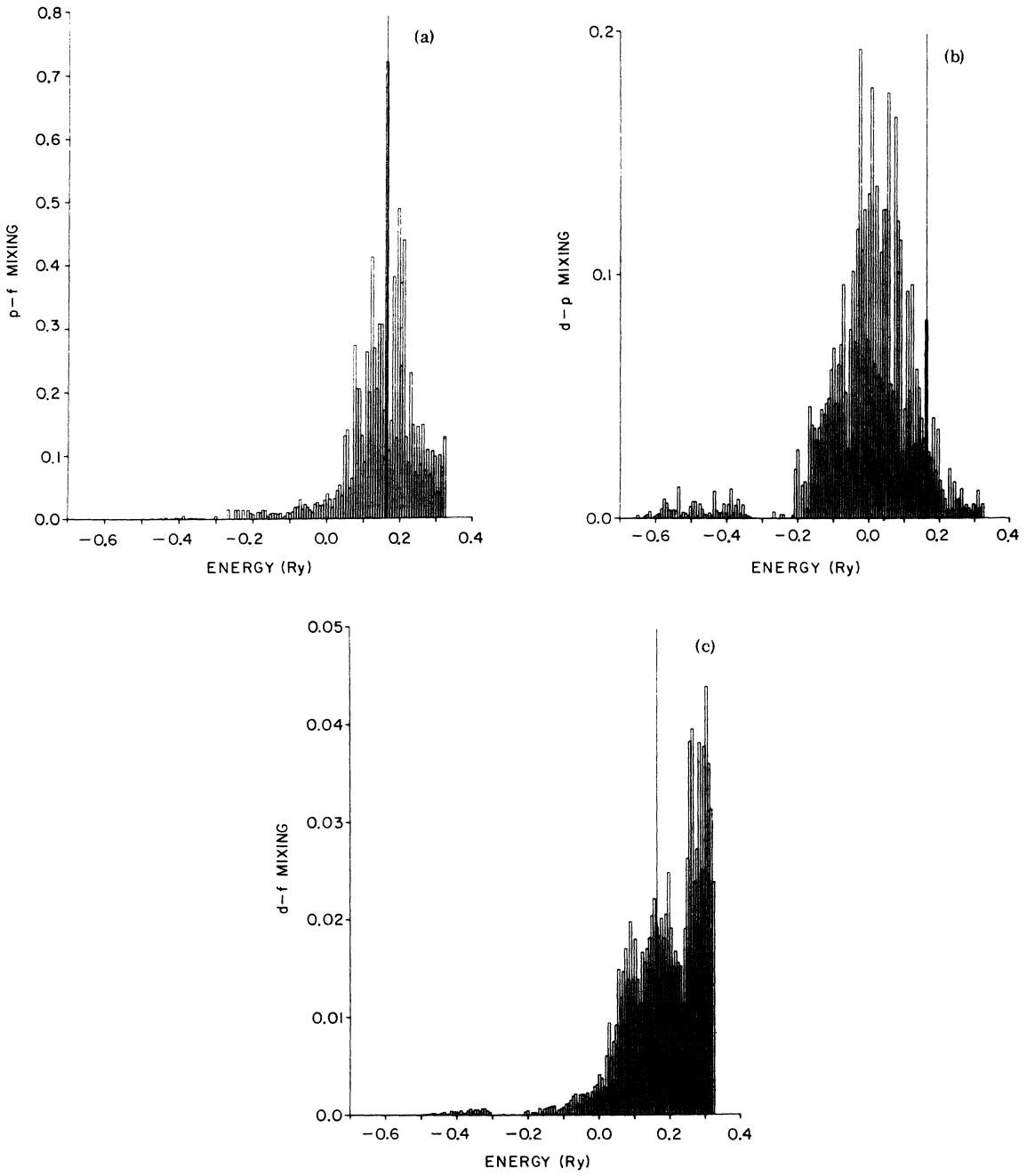

FIG. 8. Mixing of various wave-function character found in the wave functions. The parameters $\xi_{\nu\nu'}$ defined in the text are shown for (a) U-*f*, Ge-*p*; (b) U-*d*, Ge-*p*; and (c) U-*d*, U-*f* character.

electronic structure of UGe_3. This has emboldened us to try piecing together the behavior of the entire class of compounds. This may even work as well for the Np compounds.

ACKNOWLEDGMENT

This work supported in part by the U. S. Department of Energy.

[1]*The Actinides: Electronic Structure and Related Properties*, edited by A. J. Freeman and J. B. Darby, Jr. (Academic, New York, 1974); see Chap. 4 on the crystal emistry by D. J. Lam, J. B. Darby, Jr., and M. v. Nevitt.
[2]M. H. van Maaren, H. J. van Daal, and K. H. J. Buschow, Solid State Commun. 14, 145 (1974).
[3]K. H. J. Buschow and H. J. van Daal, AIP Conf. Proc. 5, 1464 (1971).
[4]M. B. Brodsky (private communication).
[5]A. Misuik, J. Mulak, A. Czopnik, and W. Trzebiatowski, Bull. Acad. Pol. Sci., Ser. Sci. Chim. 20, 337 (1972).
[6]H. H. Hill, Nucl. Met. 17, 2 (1970).
[7]A. J. Arko, M. B. Brodsky, G. W. Crabtree, D. Karim, D. D. Koelling, and L. R. Windmiller, Phys. Rev. B 12, 4102 (1975).
[8]D. D. Koelling and A. J. Freeman, *Plutonium 1975 and Other Actinides*, edited by H. Blank (North-Holland, Amsterdam, 1976), p. 291.
[9]A. J. Arko, M. B. Brodsky, G. W. Crabtree, D. Karim, L. R. Windmiller, and J. B. Ketterson, in Ref. 8, p. 325.
[10]D. D. Koelling, *Proceedings of the Second International Conference on the Electronic Structure of the Actinides*, edited by J. Mulak, W. Suski, and R. Troc (Ossolineum, Wroclaw, Poland, 1977), p. 295.
[11]A. J. Arko, in Ref. 10, p. 309.
[12]J. C. Slater, *Quantum Theory of Molecules and Solids*, Vol. II (McGraw-Hill, New York, 1965) (see Table 3.1).
[13]R. W. Stark and L. R. Windmiller, Cryogenics 8, 272 (1968).
[14]G. F. Brennert, W. A. Reed, and E. Fawcett, Rev. Sci. Instrum. 36, 1267 (1965).
[15]L. R. Windmiller, J. B. Ketterson, and J. C. Shaw, Report No. ANL-7907 (National Technical Information Service, U. S. Department of Commerce, Washington, D.C., 1972).
[16]A. J. Arko and D. D. Koelling, AIP Conf. Proc. 34, 227 (1976).
[17]J. A. Gerber, D. J. Sellmeyer and A. J. Arko, J. Low Temp. Phys. 29, 345 (1977).
[18]D. D. Koelling and G. O. Arbman, J. Phys. F 5, 2041 (1975).
[19]O. K. Andersen, Phys. Rev. B 12, 3060 (1975).
[20]O. Gunnarsson, B. I. Lundqvist, and J. W. Wilkins, Phys. Rev. B 10, 1319 (1974); and O. Gunnarsson and B. Lundqvist, *ibid.* 13, 4274 (1976).
[21]L. Hodges, R. E. Watson, and H. Ehrenreich, Phys. Rev. B 5, 3953 (1972).
[22]O. K. Andersen, Solid State Commun. 13, 133 (1973).
[23]J. C. Slater, in Ref. 12, Chap. 4, and Quarterly Progress Report of the Solid State and Molecular Theory Group, MIT, Vol. 54, p. 4 (1964) (unpublished).
[24]J. P. van Dyke (unpublished).
[25]D. D. Koelling, D. E. Ellis, and R. J. Bartlett, J. Chem. Phys. 65, 3331 (1976).

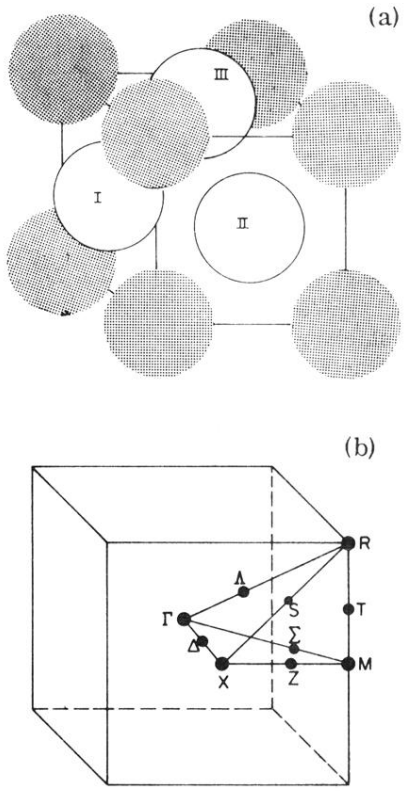

FIG. 1. $L1_2$ (Cu_3Au type) crystal structure (a) and Brillouin zone (b). The Cu_3Au structure can easily be visualized as a face-centered-cubic lattice in which the face-centered sites (I, II, and III) are occupied by Cu and the simple cubic (i.e., corner) sites are occupied by Au.

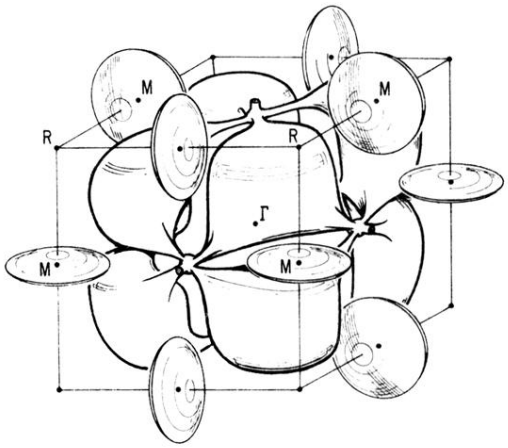

FIG. 3. Proposed topology of the electron Fermi surfaces.

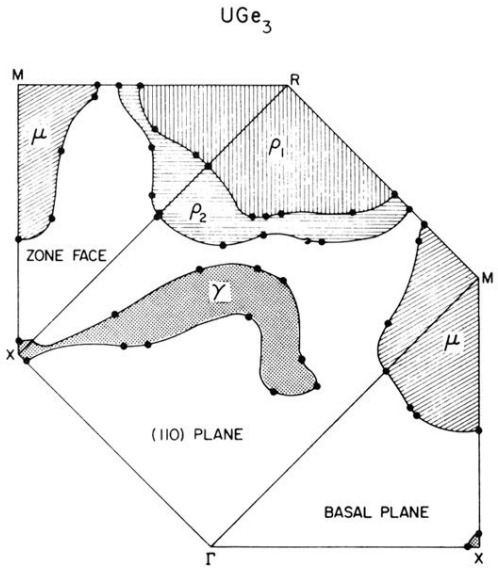

FIG. 7. Intersection of the calculated Fermi surface with the planes bounding the $\frac{1}{48}$th of the Brillouin zone shown in Fig. 1.